Creation of Solitons and Vortices by Bragg Reflection of Bose-Einstein Condensates in an Optical Lattice

R. G. Scott,[1] A. M. Martin,[1] T. M. Fromhold,[1] S. Bujkiewicz,[1,2] F. W. Sheard,[1] and M. Leadbeater[3]

[1]*School of Physics and Astronomy, University of Nottingham, Nottingham NG7 2RD, United Kingdom*
[2]*Institute of Physics, Wrocław University of Technology, Wybrzeże Wyspiańskiego 27, 50-370 Wrocław, Poland*
[3]*Department of Physics, University of Durham, South Road, Durham DH1 3LE, United Kingdom*

We study the dynamics of Bose-Einstein condensates in an optical lattice and harmonic trap. The condensates are set in motion by displacing the trap and initially follow simple semiclassical paths, shaped by the lowest energy band. Above a critical displacement, the condensate undergoes Bragg reflection. For high atom densities, the first Bragg reflection generates a train of solitons and vortices, which destabilize the condensate and trigger explosive expansion. At lower densities, soliton and vortex formation requires multiple Bragg reflections, and damps the center-of-mass motion.

Optical lattices (OLs) provide unprecedented control of transport through the energy bands of periodic quantum systems. This has led to experimental demonstrations of Bloch oscillations [1] and quantized Wannier-Stark ladders [2] for noninteracting ultracold alkali atoms. There is also great interest in understanding the behavior of Bose-Einstein condensates (BECs), formed from interacting alkali atoms, in OLs [3–16]. Predictions [4,5] that accelerated BECs will perform Bloch oscillations, whose turning points at the top of the energy band correspond to successive Bragg reflections, have been confirmed in experiments [7,12] on ^{87}Rb BECs with equilibrium peak densities $n_0 \lesssim 10^{14}$ cm^{-3}. For $n_0 \gtrsim 10^{14}$ cm^{-3}, more complex motion has been observed [11,12], which cannot be explained by Bragg reflection or analogous semiclassical models of energy band transport. Previous numerical studies of condensate dynamics in OLs have used one-dimensional (1D) and three-dimensional (3D) Gross-Pitaevskii equations [5,8,11,16]. They provide invaluable insights for understanding the center-of-mass motion of the BEC, but have not related this motion to changes in the *internal* structure of the atom cloud, in particular, dynamical excitations such as solitons and vortices. Producing such excitations in a controlled way requires state-of-the-art experimental techniques, which involve manipulating the phase and/or density profile of the BEC [15,17–20], rotating the confining trap [21,22], moving a laser beam through the atom cloud [13,23,24], or tuning the interatomic interactions [25].

In this Letter, we show that Bragg reflection provides a new mechanism for generating solitons and vortices in BECs [26]. Moreover, these excitations can have a dramatic effect on the evolution of the atom cloud. At the first Bragg reflection, the condensate wave function is a standing wave with nodes at each maximum in the OL potential. At each node, the condensate phase changes abruptly by π. Bragg reflection therefore imprints atom density and phase profiles similar to those used to generate sol-

itons in experiment [15,17–20]. The effect of this imprinting on the condensate dynamics depends critically on the atom density. For condensates with $n_0 \gtrsim 10^{14}$ cm^{-3}, realized in recent experiments [11,12], it leads to the self-assembly of a chain of stationary solitons, which decay rapidly into vortex rings. Strong interactions between the vortices destabilize the atom cloud, causing it to explode and fragment. For $n_0 \lesssim 10^{14}$ cm^{-3}, the standing wave formed at the first Bragg reflection produces no dynamical excitations. But subsequent Bragg reflections do generate solitons and vortices, which damp the center-of-mass motion. The dissipation and instability processes that we identify could play a key role in the complex dynamics recently observed for high-density condensates in OLs [11,12].

We consider condensates formed from N_A ^{87}Rb atoms in a 1D OL and a 3D harmonic trap, which is symmetrical under rotation about the OL (x) axis [27]. The potential energy profile of the OL is $V_{OL}(x) = V_0 \sin^2(\pi x/d)$. As in recent experiments [11], $d = 397.5$ nm and $V_0 = h \times 5.6$ kHz $= 1.53 E_R$, where E_R is the recoil energy. The confining potential energy is $V(x, r) = V_{OL}(x) + \frac{1}{2}m(\omega_x^2 x^2 + \omega_r^2 r^2)$, where r is the radial coordinate, m is the mass of a single atom, and ω_x, ω_r are frequencies of the harmonic trap. For most of the results presented here, $\omega_x = 2\pi \times 50$ rad s^{-1}, $\omega_r = 2\pi \times 35$ rad s^{-1}, $N_A = 1.2 \times 10^4$, and $n_0 = 0.43 \times 10^{14}$ cm^{-3} (system A). We also consider a second set of parameters, $\omega_x = 2\pi \times 8.7$ rad s^{-1}, $\omega_r = 2\pi \times 90$ rad s^{-1}, and $N_A = 3 \times 10^5$ (system B), corresponding to recent experiments [11]. In this case, n_0 is sufficiently high ($\sim 1.5 \times 10^{14}$ cm^{-3}) for the standing wave formed during Bragg reflection to have a particularly dramatic effect on the BEC. For both sets of parameters, ω_x is small enough to ensure that the harmonic potential energy variation across each OL period is much less than the width $\Gamma = h \times 2.4$ kHz $= 0.67 E_R$ of the lowest energy band. Consequently, the harmonic trap only weakly perturbs the band structure [28].

We determine the 3D density profile of the condensate ground state by using the Crank-Nicolson method [5] to solve the time-dependent Gross-Pitaevskii equation

$$i\hbar\frac{\partial\Psi}{\partial t} = \left[\frac{-\hbar^2}{2m}\nabla^2 + V(x,r) + \frac{4\pi a\hbar^2}{m}|\Psi|^2\right]\Psi, \quad (1)$$

where ∇^2 is the Laplacian in cylindrical coordinates, $a = 5.4$ nm is the s-wave scattering length [29], and $\Psi(x,r,t)$ is the axially symmetrical condensate wave function [16], normalized so that $|\Psi|^2$ is the number of atoms per unit volume. The equilibrium density profile of system A is shown in Fig. 1(a).

At $t = 0$, we disrupt the equilibrium by suddenly displacing the harmonic potential through a distance Δx along the x axis [11]. This increases the initial potential energy of the BEC by $\Delta V \simeq \frac{1}{2}m\omega_x^2(\Delta x)^2$ [Fig. 1(b)]. As the atoms start to move, this potential energy is converted into kinetic energy, which determines how far the BEC accelerates up the lowest energy band [28]. In order for the condensate to reach the top of the band and therefore undergo Bragg reflection, ΔV must be $\geq \Gamma$, which, for system A, requires $\Delta x \geq (2\Gamma/m\omega_x^2)^{1/2} = 15$ μm.

We now consider the condensate dynamics obtained from Eq. (1) for $\Delta x = 10$ μm, below the threshold for Bragg reflection. Figure 2(a) shows that the mean (center-of-mass) position of the BEC, $\langle x\rangle$, undergoes simple periodic motion, bounded by the harmonic trap. The internal structure of the BEC is unaffected by this motion, being the same at $t = 10.7$ ms [Fig. 2(a) left inset] and $t = 21.3$ ms [Fig. 2(a) right inset] as at $t = 0$. To determine how the BEC moves in reciprocal space, we calculate the Fourier transform of $\Psi(x,0,t)$. The Fourier power, $|f(k_x,t)|^2$, corresponding to wave number k_x, remains narrow and changes periodically as t increases [grey-scale plot in Fig. 2(b)]. Since the BEC's internal structure does not change with t when $\Delta x = 10$ μm, the form of $|f(k_x,t)|^2$ and the corresponding $\langle x\rangle$ versus t curve [Fig. 2(a)] can be understood by considering the motion of a point particle in the lowest energy band. The single-particle trajectories $x(t)$ and $k_x(t)$ in real and reciprocal space are determined by the semiclassical equations of motion $dx/dt = \hbar^{-1}dE(k_x)/dk_x$ and $dk_x/dt = \hbar^{-1}F_x$
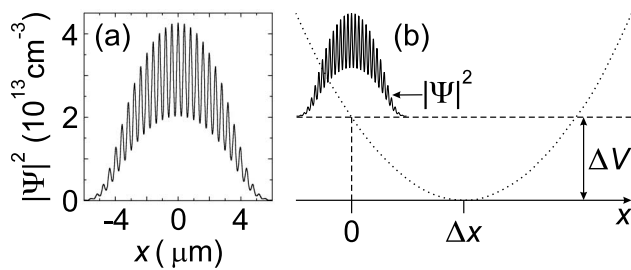
[30], where $E(k_x)$ is the energy-wave-number dispersion relation for the band, and $F_x = -m\omega_x^2 x$ is the restoring force along the x axis. In Fig. 2(b), the Fourier power (grey-scale plot) is concentrated along the single-particle $k_x(t)$ curve (white circles). The corresponding real-space trajectory, $x(t)$, is indistinguishable from the plot of $\langle x\rangle$ versus t shown in Fig. 2(a).

When Δx is increased to 25 μm, above the threshold for Bragg reflection, the mean x position of the BEC, determined from Eq. (1), performs damped periodic motion [solid curve in Fig. 2(c)]. In Fig. 2(d), the grey-scale plot of $|f(k_x,t)|^2$ shows that the BEC's mean k_x value increases approximately linearly with t and reaches the Brillouin zone boundary at 2.6 ms. At this time, the BEC undergoes Bragg reflection, which produces the first (arrowed) turning point in Fig. 2(c). The quantum calculations of $\langle x\rangle$ and $|f(k_x,t)|^2$ deviate rapidly from the
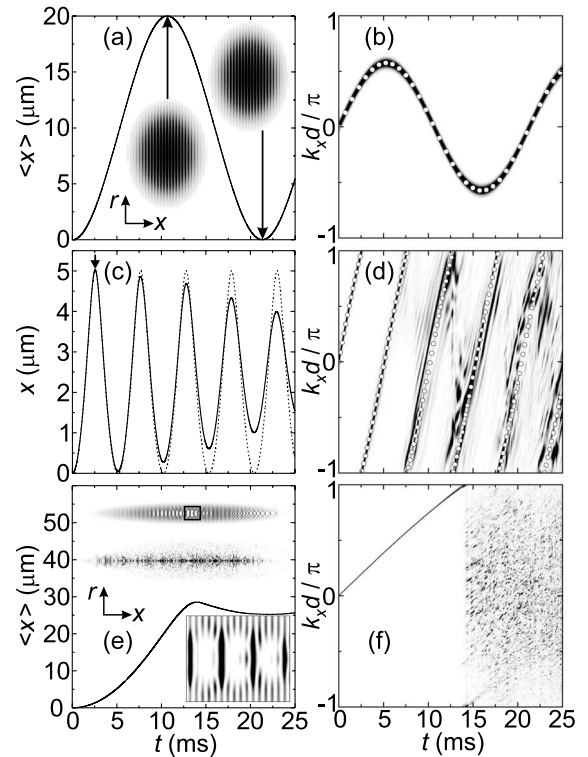
FIG. 2. (a) $\langle x\rangle$ versus t for system A with $\Delta x = 10$ μm. Insets: grey-scale plots of density (black = high) in the x-r plane (axes inset) at $t = 10.7$ ms (left) and 21.3 ms (right). (b) Grey-scale plot: $|f(k_x,t)|^2$ (white = 0, black = high) for system A with $\Delta x = 10$ μm. Open circles: points on semiclassical trajectory $k_x(t)$. (c) Solid curve: $\langle x\rangle$ versus t for system A with $\Delta x = 25$ μm. The arrow marks the first turning point. Dashed curve: semiclassical orbit $x(t)$. (d) Same as (b), but for $\Delta x = 25$ μm. (e) $\langle x\rangle$ versus t for system B with $\Delta x = 150$ μm. Insets: grey-scale plots of density (black = high) in the x-r plane at $t = 13.8$ ms (top) and 18 ms (middle). The lower inset shows an enlargement of the boxed region in the upper inset. (f) Same as (b), but for system B with $\Delta x = 150$ μm and omitting the $k_x(t)$ curve which, for $t \lesssim 13$ ms, is indistinguishable from the narrow Fourier distribution.

FIG. 1. (a) Initial atom density profile of system A, along $r = 0$. (b) Density profile and x dependence of harmonic potential energy (dotted line) immediately after trap displacement.

corresponding semiclassical trajectories, $x(t)$ and $k_x(t)$, shown, respectively, by the dashed curve and open circles in Figs. 2(c) and 2(d). For $t \gtrsim 7.5$ ms, the oscillations in $\langle x \rangle$ are damped and multiple peaks appear in $|f(k_x, t)|^2$, which spreads throughout the Brillouin zone. This deviation from single-particle behavior indicates that the BEC's center-of-mass motion is strongly affected by changes in its internal structure. Key stages in the evolution of the density profile are shown in Fig. 3. As t increases from zero [Fig. 3(a)], the density minima deepen and fall to zero at the first Bragg reflection, which we now analyze.

The lower curves in Figs. 4(a)–4(c) show $|\Psi(x, 0, t)|^2$ just before ($t = 2$ ms), at ($t = 2.6$ ms), and just after ($t = 3$ ms) the first Bragg reflection. The upper curves show the wave function phase, $\phi(x)$, modulo 2π. Just before reflection [Fig. 4(a)], the density near the center of the BEC has a minimum value of $\sim 10^{13}$ cm^{-3}, which is approximately half that at $t = 0$ (Fig. 1). The local velocity along the x direction, $v_x = (\hbar/m)d\phi/dx$, is > 0 throughout the BEC. At the point of Bragg reflection [Fig. 4(b)], the density minima fall to zero at each peak in $V_{OL}(x)$. At each zero, ϕ changes abruptly by π [upper curve in Fig. 4(b)]. Away from the discontinuities, $d\phi/dx \simeq 0$, indicating that the BEC is at rest. This variation of density and phase demonstrates that a standing wave forms during Bragg reflection. In recent experiments, laser illumination was used to produce individual density minima and π phase shifts [15,17–20], which subsequently evolved into dark solitons. By analogy, the standing wave might be expected to generate a chain of stationary solitons each of width $w \approx (2\pi a n_M)^{-1/2}$, where n_M is the local mean atom density [19]. At the first Bragg reflection, $n_M \simeq 3 \times 10^{13}$ cm^{-3} near the center of the BEC in system A [see Fig. 4(b)], and so $w \simeq 2.5d$. Since w is much larger than the width ($\sim d$) of the density minima in the standing wave, the first Bragg reflection does not produce solitons in system A. Instead, after reflection, the density minima rise away from zero and $d\phi/dx$ becomes negative for all x [Fig. 4(c)], as the BEC starts to move from right to left.
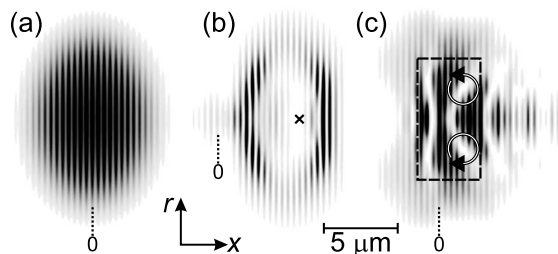
We now consider the condensate motion for $t \gtrsim 5$ ms. Figure 3(b) shows the density profile at the second Bragg reflection, when $t = 7.8$ ms. Again a standing wave is formed, which creates nodal planes in the density profile [white stripes in Fig. 3(b)] at each maximum in $V_{OL}(x)$. However, in contrast to the first Bragg reflection, the standing wave now disrupts the internal structure of the condensate sufficiently to allow a soliton, marked by the cross in Fig. 3(b), to form across several OL periods. Subsequent Bragg reflections generate more solitons, which have a pronounced effect on the condensate's internal structure and center-of-mass motion. To illustrate this, Fig. 3(c) shows the density profile at $t = 10.9$ ms. For $x < 0$, there is an extended soliton (white crescent shape), whose wave front has been curved by refraction originating from the nonuniform density [13]. This refraction is the precursor of snake instability [13], which causes the solitons to decay into vortex rings. When viewed in a two-dimensional (x, r) cross section, each vortex ring appears as two vortices with opposite circulation, such as those enclosed by arrows in Fig. 3(c). At the center of each vortex, $|\Psi|^2 = 0$. The vortices can be seen more clearly in Figs. 5(a) and 5(b), which show, respectively, enlargements of the density profile within the dashed box in Fig. 3(c), and the corresponding phase. At the center of the soliton represented by the white crescent in Fig. 5(a), the phase changes abruptly from $3\pi/2$ (dark grey) to $\pi/2$ (light grey) as x increases. Around the two vortices, the phase [Fig. 5(b)] changes continuously from 0 (white) to 2π (black), indicating quantized circulation in the direction of the arrows. Vortex formation is the main cause of damping in the center-of-mass motion [Fig. 2(c)]. A crucial aspect of this damping mechanism is that the soliton formation and subsequent vortex shedding occur when the condensate is almost *at rest*. It is therefore *fundamentally different* from the phonon emission process used to interpret experiments on system B [11], which occurs when v_x exceeds a critical value of ~ 5 mm s^{-1}. It is also unrelated to the damping found in 1D simulations of Bloch-oscillating condensates [31], which cannot include the effects of vortex formation. We now relate our calculations to experiments on system B [11]. Figures 2(e) and 2(f) show the time evolution of $\langle x \rangle$ and $|f(k_x, t)|^2$ for this system, after a large
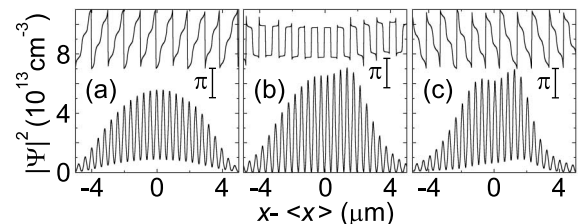

FIG. 3. Grey-scale plots of density (white = 0, black = high) in the x-r plane (axes inset) for system A with $\Delta x = 25$ μm and $t = 0$ ms (a), 7.8 ms (b), 10.9 ms (c). Vertical dotted lines indicate $x = 0$ in each case. The horizontal bar shows scale. The cross in (b) marks the center of a soliton. The region within the dashed box in (c) is shown in Fig. 5(a).

FIG. 4. Lower curves: density profiles along $r = 0$ for the condensate in system A with $\Delta x = 25$ μm and $t = 2$ ms (a), 2.6 ms (b), 3 ms (c). Upper curves show $\phi(x)$ modulo 2π, with vertical scale indicated by bars of length π.
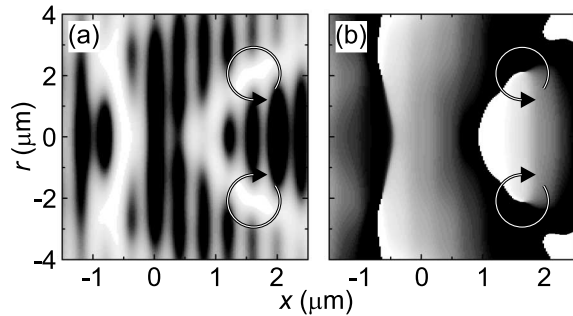
FIG. 5. (a) Grey-scale plot of density for system A within the dashed box in Fig. 3(c) (white = 0, black = high). Arrows show the direction of circulation around vortices. (b) Grey-scale plot of ϕ (white = 0, black = 2π).

trap displacement of 150 μm. As in system A, the first Bragg reflection generates a density node and a π phase shift at each maximum in $V_{OL}(x)$. But since n_M is much larger in system B ($\sim 1.6 \times 10^{14}$ cm^{-3} near the BEC center at the first Bragg reflection), $w \simeq d$. Since w is so closely matched to the width of the density minima in the standing wave, Bragg reflection causes the self-assembly of ~10 stationary solitons, which form a chain across the central third of the BEC. Figure 2(e) shows the compact cigar-shaped density profile of the BEC just after the first Bragg reflection (upper inset). The region within the box is shown enlarged in the lower inset of Fig. 2(e), which reveals three stationary solitons (extended white areas). The time taken for solitons to develop following phase imprinting is proportional to the distance l over which the phase changes by π [15]. In a standing wave, $l \simeq 0$, and so the first Bragg reflection and the formation of the soliton chain occur almost instantaneously. The solitons decay rapidly into a chain of vortex rings, which form a complex interacting system. The interactions create a large internal strain, which causes the BEC to explode radially, resulting in the diffuse and fragmented atom density profile shown in the middle inset of Fig. 2(e) [32]. The explosion has a dramatic effect on the k_x distribution of the atoms [Fig. 2(f)], which is initially extremely narrow but, at the point of Bragg reflection, spreads throughout the Brillouin zone. This could account for the broad momentum distribution observed when high-density BECs undergo Bragg reflection [12].

In summary, we have investigated how Bragg reflection affects the internal structure and center-of-mass motion of condensates accelerating through an OL. When the atom density is high enough to ensure that $w \lesssim d$, the density zeros and π phase shifts imprinted by the first Bragg reflection generate a train of stationary solitons, which decay rapidly into vortex rings. Strong interactions between the ensemble of vortices have a catastrophic effect on the condensate, causing it to undergo explosive expansion. This dynamical regime is a unique feature of condensates in an OL and should be experimentally accessible in existing systems [11,12]. For

lower atom densities, soliton formation requires multiple Bragg reflections. The subsequent decay of the solitons into vortex rings provides a new dissipation mechanism, which could contribute to the damping of the center-of-mass oscillations observed in experiment [11].

[1] M. Ben Dahan *et al.*, Phys. Rev. Lett. **76**, 4508 (1996).
[2] S. R. Wilkinson *et al.*, Phys. Rev. Lett. **76**, 4512 (1996).
[3] D. Jaksch *et al.*, Phys. Rev. Lett. **89**, 040402 (2002); **81**, 3108 (1998).
[4] K. Berg-Sørensen and K. Mølmer, Phys. Rev. A **58**, 1480 (1998).
[5] D. I. Choi and Q. Niu, Phys. Rev. Lett. **82**, 2022 (1999).
[6] K. P. Marzlin and W. Zhang, Phys. Rev. A **59**, 2982 (1999).
[7] B. P. Anderson and M. A. Kasevich, Science **282**, 1686 (1998).
[8] M. Holthaus, J. Opt. B: Quantum Semiclassical Opt. **2**, 589 (2000).
[9] F. S. Cataliotti *et al.*, Science **293**, 843 (2001).
[10] J. C. Bronski *et al.*, Phys. Rev. Lett. **86**, 1402 (2001).
[11] S. Burger *et al.*, Phys. Rev. Lett. **86**, 4447 (2001).
[12] O. Morsch *et al.*, Phys. Rev. Lett. **87**, 140402 (2001).
[13] Z. Dutton *et al.*, Science **293**, 663 (2001).
[14] M. Greiner *et al.*, Phys. Rev. Lett. **87**, 160405 (2001); Nature (London) **415**, 39 (2002).
[15] S. Burger *et al.*, Phys. Rev. A **65**, 043611 (2002).
[16] M. L. Chiofalo and M. P. Tosi, Phys. Lett. A **268**, 406 (2000).
[17] M. R. Matthews *et al.*, Phys. Rev. Lett. **83**, 2498 (1999).
[18] S. Burger *et al.*, Phys. Rev. Lett. **83**, 5198 (1999).
[19] J. Denschlag *et al.*, Science **287**, 97 (2000).
[20] B. P. Anderson *et al.*, Phys. Rev. Lett. **86**, 2926 (2001).
[21] K.W. Madison *et al.*, Phys. Rev. Lett. **84**, 806 (2000).
[22] J. R. Abo-Shaeer *et al.*, Science **292**, 476 (2001).
[23] C. Raman *et al.*, Phys. Rev. Lett. **83**, 2502 (1999).
[24] B. Jackson *et al.*, Phys. Rev. A **61**, 051603(R) (2000).
[25] K. E. Strecker *et al.*, Nature (London) **417**, 150 (2002).
[26] As in [19] and in C. J. Pethick and H. Smith, *Bose-Einstein Condensation in Dilute Gases* (Cambridge University Press, Cambridge, 2002), we take the term *soliton* to be synonymous with *solitary wave*.
[27] For given n_0, we obtain similar results for two-dimensional BECs that are strongly confined in one direction normal to the x axis.
[28] R. G. Scott *et al.*, Phys. Rev. A **66**, 023407 (2002).
[29] E. A. Burt *et al.*, Phys. Rev. Lett. **79**, 337 (1997).
[30] See, for example, N.W. Ashcroft and N. D. Mermin, *Solid State Physics* (Holt, Rinehart, and Winston, Philadelphia, 1976).
[31] A. Trombettoni and A. Smerzi, Phys. Rev. Lett. **86**, 2353 (2001).
[32] Dynamical instabilities have been demonstrated for 1D models of BECs in OLs by B. Wu and Q. Niu, Phys. Rev. A **64**, 061603 (2001); F. Kh. Abdullaev *et al.*, Phys. Rev. A **64**, 043606 (2001). In contrast, the vortex-induced explosion shown in Fig. 2(e) cannot occur in 1D.

Author/s:
Scott, RG; Martin, AM; Fromhold, TM; Bujkiewicz, S; Sheard, FW; Leadbeater, M

Title:
Creation of solitons and vortices by Bragg reflection of Bose-Einstein condensates in an optical lattice

Date:
2003-03-21

Citation:
Scott, R. G., Martin, A. M., Fromhold, T. M., Bujkiewicz, S., Sheard, F. W. & Leadbeater, M. (2003). Creation of solitons and vortices by Bragg reflection of Bose-Einstein condensates in an optical lattice. PHYSICAL REVIEW LETTERS, 90 (11), https://doi.org/10.1103/PhysRevLett.90.110404.

Persistent Link:
http://hdl.handle.net/11343/43073